Journal of Low Temperature Physics (2023) 210:325–333
https://doi.org/10.1007/s10909-022-02863-0

The Inverse Magnetocaloric Effect of MgB_2 Superconductor

Youssef H. Abdelalim[1] · Ashraf M.Mohamed[2] · Mahmoud A. Hamad[3] · Hatem R. Alamri[4] · Mohamed E. Harb[5] · Sameh M. Elghnam[6]

Received: 10 April 2022 / Accepted: 30 August 2022 / Published online: 8 October 2022

Abstract
The magnetocaloric effect-(MCE) of MgB_2 is simulated, considering the effect of sintering temperature on MCE. The results show that MCE of MgB_2 samples is an inverse type in a temperature range of diamagnetic-paramagnetic transition. Moreover, the MCE for MgB_2 is improved with high sintering temperature. The comparison between MCE of MgB_2 samples and other some reported magnetic materials has been done, showing that MCE parameters of MgB_2 samples are larger than some MCE parameters of $La_{1-x}Cd_xMnO_3$, $La_{1.25}Sr_{0.75}MnCoO_6$, $Gd_{1-x}Ca_xBaCo_2O_{5.5}$, $Ni_{58}Fe_{26}Ga_{28}$, $Ni_{2+x}Mn_{1-x}Ge$, $Ge_{0.95}Mn_{0.05}$ film, and (001)-oriented MnAs film. It suggested that MgB_2 samples could be a promising sharing candidate for MR in cryogenic temperatures.

Keywords Magnetocaloric effect · Phenomenological model · MgB_2

1 Introduction

The magnetic refrigerator (MR) has become very important as an alternative to gas refrigerator because of its low consumption of electricity, more environmentally friendly device, lower noise, and larger efficiency in the process of cooling [1–7].

✉ Hatem R. Alamri
hriamri@uqu.edu.sa

Mahmoud A. Hamad
m_hamad76@yahoo.com

1 Alexandria University, Alexandria, Egypt

2 Applied Organic Chemistry Department, National Research Centre, Dokki, Cairo 12622, Egypt

3 Basic Science Department, Higher Institute of Engineering and Technology, Alexandria, Egypt

4 Physics Department, Aljamoum University College, Umm Al-Qura University, Makkah 21955, Saudi Arabia

5 Department of Computer Science, Higher Institute of Computer and Information Systems-Abou Qir, Alexandria, Egypt

6 Physics Department, Faculty of Science, Alexandria University, Alexandria, Egypt

The basic idea of MR depends on using the magnetocaloric effect-(MCE) in the magnetic materials [7–9]. This MCE is an effect that occurs upon a sudden change in the applied magnetic field (ΔH) and is followed by a change in magnetic entropy change (ΔS_M) and temperature [8–14]. Subsequently, it is thought that the efficiency of MR can be enhanced by functioning many types of magnets, having MCE at cryogenic and room temperatures such as magnetic alloys, magnetic composites, ferrites, manganites, rare earth-based materials, and other types [15–19].

In a usual MCE, the cooling operation in magnetic material occurs as a result of adiabatic demagnetization that is done by removing the applied magnetic field [20]. Conversely, the magnetic materials can be cooled via the adiabatic magnetization that is done by increasing the external magnetic field. This effect is named inverse MCE [21]. This inverse MCE can occur in superconductors over the temperature range of the diamagnetic-paramagnetic transition. Therefore, it is recommended to use different types of superconductors over various temperature ranges of the diamagnetic-paramagnetic transition in the cryogenic system.

Since the detection of MgB_2 as a metallic superconductor material with a transition temperature (T_{trans}) of 39 K, there are extreme efforts to detect its performance and improve its physical properties [22–24].

MgB_2 is used in many significant applications like magnets due to its high proficiency that allows it to trap magnetic fields more than different types of ferromagnets and T_{trans} of 39 K, creating it as a practical material for exploiting in the cryogenic system and superconducting magnets for accelerators and superconducting motors in electric aircraft [25]. Furthermore, MgB_2 is very important in magnetic resonance imaging-(MRI) systems without using liquid helium (LHe), because the price of LHe is increased rapidly in recent years, causing the MRI system to be very expensive [26]. Yudanto et al. prepared MgB_2 superconductors by mechanical alloying at various sintering temperatures, revealing that the content percentage of MgB_2 phase in the prepared sample is enhanced and more than 90% in samples sintered at temperatures of 850 °C and 900 °C [27]. Furthermore, they have revealed that the behavior of MgB_2 as a superconductor was enhanced in samples sintered at temperatures of 850 °C and 900 °C. From these noteworthy results, its purpose is to investigate the MCE of MgB_2 in this work. In this research, a phenomenological model (PM) was used to deduce the thermomagnetic properties of MgB_2 by simulating the *M(T)* curves, concluding ΔS_M, heat capacity change ($\Delta C_{P,H}$), and relative cooling power (RCP).

2 Theoretical Aspects of MCE

According to PM [28–32], the magnetization (M) versus temperature (T) of MgB_2 through the magnetic transition can be simulated by:

$$M = \frac{\Delta M}{2}\left[\tanh(A(T_{trans} - T))\right] + BT + C \quad (1)$$

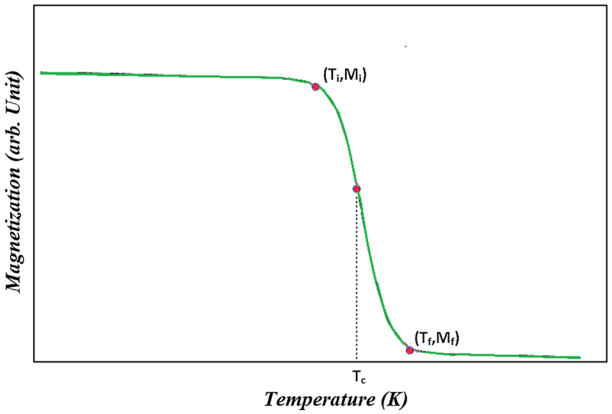

Fig. 1 Temperature dependence of magnetization in constant applied field

where, $\Delta M = M_i - M_f$ (M_i and M_f are the initial and final values of the magnetization at the diamagnetic-paramagnetic transition region, respectively, as shown in Fig. 1), $A = \frac{2(B-S_c)}{\Delta M}$, B is the average of $(\frac{dM}{dT})$ at diamagnetic state, S_c is the maximum value of $\frac{dM}{dT}$ and $C = (\frac{M_i+M_f}{2}) - BT_{\text{trans}}$. In this work, we can observe $M_f \approx 0$. Then $\Delta M = M_i$.

3 Results and Discussion

The open symbols and solid lines indicate the experimental data of *M(T)* curves for MgB_2 in Ref. [27] and the simulated data using Eq. (1), respectively. The MgB_2 samples that were sintered at temperatures of 700, 800, 850, and 900 °C are named MB600, MB700, MB800, MB850, and MB900, respectively, as depicted in Fig. 2.

There is a convincing agreement between the experimental and simulated *M(T)* for MgB_2 under 0.01 T magnetic field, deducing that PM is a suitable model for fitting *M(T)* curves for MgB_2. MgB_2 displays a sharp transition from the diamagnetic state to the paramagnetic state. This sharp transition allows the ΔS_M value of MgB_2 to be maximized but it is covering low-temperature range. This ΔS_M of MgB_2 under an adiabatic magnetic field shift of 0.01 T can be evaluated as follows [28, 29]:

$$\Delta S_M = 0.01\left(-\frac{M_i}{2}A\ \text{sech}^2(A(T_{\text{trans}} - T)) + B\right) \tag{2}$$

A maximum of ΔS_M (ΔS_{Max}) can be determined as follows:

$$\Delta S_{\text{Max}} = 0.01\left(-\frac{M_i}{2}A + B\right) \tag{3}$$

The rise in sintering temperature causes the particle size increase in samples due to grain growth. Also, the saturation magnetization and transition temperature

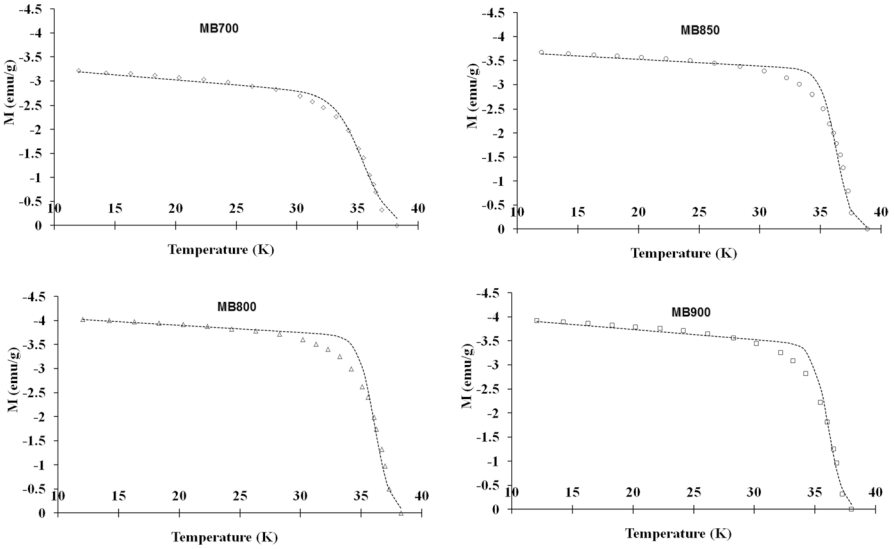

Fig. 2 Magnetization vs. temperature for MgB_2 in 0.01 T applied magnetic field

increase with a particle size which improves the magnetic properties. The T_{trans} increases with sintering temperature and the intensity of main diffraction peaks increase and FWHM decreases, clearly signifies that the crystallinity of MgB_2 is enhanced [33].

Figure 3 shows the simulated temperature dependence of ΔS_M for MgB_2 under an adiabatic magnetic field shift of 0.01 T, calculated by using Eq. (2). This diamagnetic-paramagnetic transition leads to an increase in the magnetic spin disorder causing ΔS_M and ΔS_M to reach a peak value at T_{trans}.

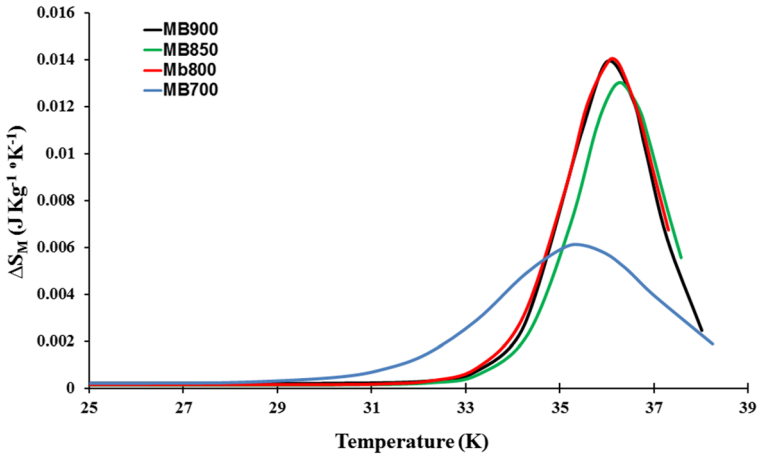

Fig. 3 ΔS_M versus temperature for MgB_2 in ΔH of 0.01 T

It is clear that the MB700 sample has the lowest value of ΔS_{Max} due to its MgO content, which is higher than the MgO content of other samples [34]. Furthermore, the MB700 sample has remarkable defects that are detected from the values of the critical temperature gap and residual resistivity ratio [35, 36]. There is a required parameter called RCP which is a measure of the ability of a material to carry heat at a relatively high-temperature difference between the hot and cold sinks in the cycle of an ideal MR. RCP of MgB_2 can be given by the ΔS_{Max} and full-width at half-maximum ($\delta \mathrm{T}_{\mathrm{FWHM}}$) of the ΔS_M curve as follows:

$$\mathrm{RCP} = \Delta S_{\mathrm{Max}}(T, H_{\mathrm{max}}) \times \delta \mathrm{T}_{\mathrm{FWHM}} \tag{4}$$

where $\delta \mathrm{T}_{\mathrm{FWHM}}$ can be obtained as follows:

$$\delta \mathrm{T}_{\mathrm{FWHM}} = \frac{2}{A} \cosh^{-1}\left(\sqrt{\frac{2AM_i}{AM_i + 2B}}\right) \tag{5}$$

In conclusion, when using different magnetic fields, magnetism and entropy will be enhanced with different calcination temperatures, which is in agreement with [37–40].

As shown in Table 1, the values of δT_{FWHM} and RCP change with sintering temperature, indicating the RCP of MgB_2 can be tailored with sintering temperature.

The behavior of the $\Delta C_{P,H}$ curve of MgB_2 under ΔH of 0.01 T can be predicted using the PM model [28–30] as follows:

$$\Delta C_{P,H} = -0.01\, TA^2 M_i\, \mathrm{sech}^2(A(T_{\mathrm{trans}} - T))\, \tanh(A(T_{\mathrm{trans}} - T)) \tag{6}$$

Figure 4 shows the simulated $\Delta C_{P,H}$ versus temperature for MgB_2 samples under $\Delta H = 0.01$ T. The simulated $\Delta C_{P,H}$ deviated from positive values to negative values around T_{trans}.

For further details, the refrigerant capacity (RC) is an important parameter to evaluate the efficiency for MgB_2 samples as effective materials in MR. RC was calculated as follows [29, 30]:

$$RC = \int_{T_C - \frac{\delta \mathrm{T}_{\mathrm{FWHM}}}{2}}^{T_C + \frac{\delta \mathrm{T}_{\mathrm{FWHM}}}{2}} \Delta S_M \mathrm{dT} \tag{7}$$

It is clear that from Table 1, $\Delta C_{P,H(\mathrm{max})}$, and RC show an increase with increasing sintering temperature. This is due to MgB_2 content going on to grow while MgO content decreases with increasing sintering temperature [27].

Table 1 shows also comparisons between MCE parameters of MgB_2 samples and corresponding ones of other compositions in previous works under low values of magnetic field variation. The MCE parameters of MgB_2 samples are significantly larger, and comparable with some MCE parameters of $La_{1\text{-}x}Cd_xMnO_3$, $La_{1.25}Sr_{0.75}MnCoO_6$, $Gd_{1-x}Ca_xBaCo_2O_{5.5}$, $Ni_{58}Fe_{26}Ga_{28}$, $Ni_{2+x}Mn_{1-x}Ge$,

Table 1 The MCE parameters for MgB_2 samples and other magnetocaloric materials in low applied magnetic field changes

Composition	ΔH (T)	$\lvert\Delta S_{Max}\rvert$ (J/kg.K)	δT_{FWHM} (K)	RCP (J/kg)	$\Delta C_{P, H(Max)}$ (J/kg.K)	RC (J/kg)	Refs.
MB700	0.01	0.006	4.2	0.025	0.06	0.01	This work
MB800	0.01	0.014	2.3	0.033	0.28	0.04	This work
MB850	0.01	0.013	2.3	0.030	0.26	0.06	This work
MB900	0.01	0.014	2.2	0.031	0.29	0.09	This work
$La_{1-x}Cd_xMnO_3$	0.05	0.011	29.65–44.03	0.326–0.484	0.087–0.105	–	[41]
$La_{1.25}Sr_{0.75}MnCoO_6$	0.5	0.0175	26–124	0.45, 2.18	0.04–0.19	–	[42]
$Gd_{1-x}Ca_xBaCo_2O_{5.5}$	0.1	1.65E-6–2.2 E-6	9.77–13.85	1.61 E-5–3.04 E-5	6.14 E-5–6.34E-5	–	[43]
$Ni_{58}Fe_{26}Ga_{28}$	0.2–0.5	0.005–0.013	42–73	0.19–0.94	0.04–0.07	–	[44]
$Ni_{2+x}Mn_{1-x}Ge$	0.05	0.019–0.02	33	0.63–0.68	0.12–0.21	–	[45]
Ge0.95Mn0.05 Films	0.1	4E-7–3.6 E-6	12.69–17.75	6.3 E-6–0.451 E-5	7.7 E-6–1.1 E-4	–	[46]
(001)-oriented MnAs films	0.03	0.01–0.02	55.47–75.50	0.07–1.22	0.07–0.083	–	[47]

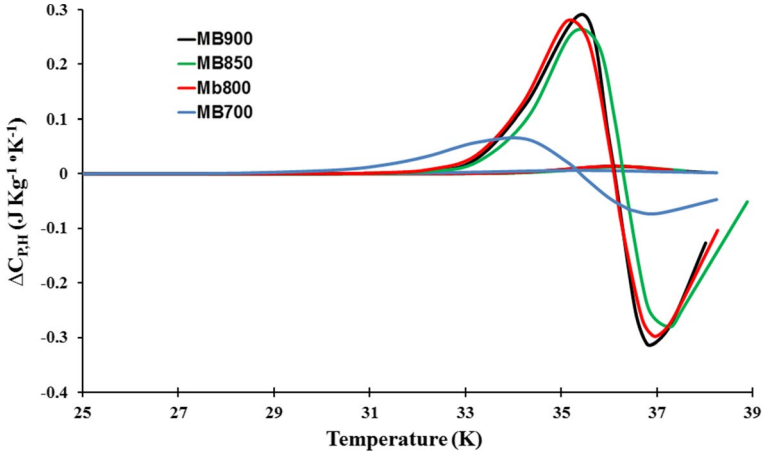

Fig. 4 $\Delta C_{P,H}$ versus temperature for MgB_2 in ΔH of 0.01 T

Ge0.95Mn0.05 Films, and (001)-oriented MnAs films as shown in Table 1 [41–47]. Finally, the combination of MCE and the electrocaloric effect creates opportunities for real-world uses of contemporary refrigeration technology [48–80].

4 Conclusion

A detailed investigation of MCE for MgB_2 samples has been done via PM, considering the effect of the sintering temperature on MCE. The results of simulation show that this PM is a valuable model for the calculation of thermomagnetic properties for MgB_2 samples in the temperature range of the diamagnetic-paramagnetic transition, confirming MCE of MgB_2 samples is of inverse type. Moreover, the MCE for MgB_2 samples is compared with those of some other reported magnetic materials, concluding that MgB_2 samples could be a promising sharing candidate for MR at cryogenic temperatures. This research will be extended in the future to optimize the magnetic properties of MgB_2 samples using a variety of external effects.

Funding Open access funding provided by The Science, Technology & Innovation Funding Authority (STDF) in cooperation with The Egyptian Knowledge Bank (EKB).

References

1. G. Kotnana, D.P. Sahu, S.N. Jammalamadaka, J. Alloys Compd. **709**, 410–414 (2017)
2. Y. Zhang, X. Xu, AIP Adv. **10**, 035220 (2020)
3. Y. Zhang, X. Xu, Appl. Phys. A **126**, 1–12 (2020)
4. S. Narayana Jammalamadaka, S.S. Rao, S.V. Bhat, J. Vanacken, V.V. Moshchalkov, J. Appl. Phys. **112**(8), 083917 (2012)
5. M.A. Hamad, O.M. Hemeda, H.R. Alamri et al., Phys. Solid State **63**, 709–713 (2021)
6. E.M. Ahmed, H.R. Alamri, S.M. Elghnam et al., Solid State **63**, 1601–1604 (2021)
7. M.A. Hamad, H.R. Alamri, J. Mater. Res. Technol. **17**, 2670–2674 (2022)
8. A.M. Ewas, M.A. Hamad, Ceram. Int. **43**, 7660–7662 (2017)
9. E.M. Ahmed, O.M. Hemeda, H.R. Alamri et al., Phase Trans. **94**, 835 (2021)
10. Y.H. Abdelalim, A.M. Mohamed, O.M. Hemeda, M.E. Harb, S.M. Elghnam, J. Magn. Magn. Mater. **560**, 169661 (2022)
11. M.A. Hamad, H.R. Alamri, J. Electron. Mater. **51**, 3359–3363 (2022)
12. Y. Zhang, X. Xu, J. Supercond. Novel Magn. **34**, 63–73 (2021)
13. Y. Zhang, X. Xu, Phys. C **592**, 1353998 (2022)
14. Y. Zhang, X. Xu, RSC Adv. **10**, 20646–20653 (2020)
15. M.A. Hamad, O.M. Hemeda, H.R. Alamri, A.M. Mohamed, Phys. Lett. A **394**, 127204 (2021)
16. M.A. Hamad, H.R. Alamri, Front. Mater. **9**, 832703 (2022)
17. A.H. El-Sayed, M.A. Hamad, Phase Trans. **92**, 517 (2019)
18. E.M. Ahmed, O.M. Hemeda, H.R. Alamri, S.M. Elghnam, M.A. Hamad, Russ. J. Phys. Chem. **96**, S101–S104 (2022)
19. M.A. Hamad, H.R. Alamri, J. Low Temp. Phys. **207**, 181–189 (2022)
20. Y. Liu, X. Zhang, D. Xing, H. Shen, D. Chen, J. Liu, J. Sun, J. Alloys Compd. **616**, 184 (2014)
21. X. Moya, L. Mañosa, A. Planes, S. Aksoy, M. Acet, E.F. Wassermann, T. Krenke, Phys. Rev. B **75**, 184412 (2007)
22. J. Nagamatsu, N. Nakagawa, T. Muranaka, Y. Zenitani, J. Akimitsu, Nature **410**, 63–64 (2001)
23. M. Tomsic, M. Rindfleisch, J. Yue, K. McFadden, J. Phillips, M.D. Sumption, M. Bhatia, S. Bohnenstiehl, E.W. Collings, Int. J. Appl. Ceram. Technol. **4**, 250–259 (2007)
24. Y. Zhang, X. Xu, Phys. C **573**, 1353633 (2020)
25. D.Y. Wang, X.F. Pan, D. Xi, Q.Y. Wang, J.Q. Feng, G. Yan, Y. Zhao, J. Supercond. Nov. Magn. **33**, 2657–2662 (2020)
26. Z. Wang, J.M. van Oort, M.X. Zou, Phys. C Supercond. Appl. **482**, 80–86 (2012)
27. S.D. Yudanto, Y.P. Dewi, A. Imaduddin, Y. Nakanishi, M. Yoshizawa, B. Kurniawan, A. Manaf, J. Supercond. Nov. Magn. **32**, 2829 (2019)
28. M.A. Hamad, Process. Appl. Ceram. **9**, 11 (2015)
29. M.A. Hamad, H.R. Alamri, J. Taibah Univ. Sci. **16**, 670–675 (2022)
30. M.A. Hamad, J. Adv. Ceram. **4**, 206–210 (2015)
31. M.A. Hamad, H.R. Alamri, J. Supercond. Nov. Magn. **35**, 515–518 (2022)
32. M.A. Hamad, J. Supercond. Nov. Magn. **28**, 173 (2015)
33. S.S. Kekade, P.A. Yadav, B.R. Thombare, P.R. Dusane, D.M. Phase, R.J. Choudhary, S.I. Patil, Mater. Res. Express **6**, 096108 (2019)
34. D.K. Singh, B. Tiwari, R. Jha, H. Kishan, V.P.S. Awana, Phys. C **505**, 104–108 (2014)
35. K.S.B. De Silva, X. Xu, S. Gambir, D.C.K. Wong, W.X. Li, Q.Y. Hu, IEEE Trans. Appl. Supercond. **23**, 1–4 (2013)
36. S. Rajput, S. Chaudhary, IEEE Trans. Appl. Supercond. **20**, 26–32 (2010)
37. G. Rivero, M. Multigner, J. Valdés, P. Crespo, A. Martínez, A. Hernando, J. Magn. Magn. Mater. **290–291**, 618–620 (2005)
38. J.R. Thompson, M. Paranthaman, D.K. Christen, K.D. Sorge, H.J. Kim, J.G. Ossandon, Supercond. Sci. Technol. **14**(5), L17–L20 (2001)
39. G. Fuchs, K.-H. Müller, A. Handstein, K. Nenkov, V. Narozhnyi, D. Eckert, L. Schultz, Solid State Commun. **118**(10), 497–501 (2001)
40. P.C. Canfield, S.L. Budko, D.K. Finnemore, Phys. Supercond. **385**(1–2), 1–7 (2003)
41. M.A. Hamad, J. Supercond. Nov. Magn. **26**, 3459 (2013)
42. M.A. Hamad, J. Therm. Anal. Calorim. **115**, 523 (2014)
43. M.A. Hamad, Mater. Lett. **82**, 181 (2012)

44. A.H. El-Sayed, M.A. Hamad, J. Supercond. Nov. Magn. **31**, 1895 (2018)
45. A.H. El-Sayed, M.A. Hamad, J. Supercond. Nov. Magn. **32**, 1447 (2018)
46. M.A. Hamad, J. Supercond. Nov. Magn. **26**, 449 (2013)
47. M.A. Hamad, J. Supercond. Nov. Magn. **27**, 263 (2014)
48. M.A. Hamad, J. Adv. Dielect. **3**, 1350029 (2013)
49. A.H. El-Sayed, M.A. Hamad, J. Supercond. Nov. Magn. **31**, 3357 (2018)
50. A.H. El-Sayed, O.M. Hemeda, M.A. Hamad, A.M. Mohamed, Eur. Phys. J. Plus **134**, 227 (2019)
51. A.H. El-Sayed, O.M. Hemeda, M.A. Hamad, A.M. Mohamed, J. Supercond. Nov. Magn. **33**, 769–773 (2020)
52. M.A. Hamad, J. Supercond. Nov. Magn. **29**, 1539 (2016)
53. M.A. Hamad, J. Supercond. Nov. Magn. **27**, 223 (2014)
54. M.A. Hamad, O.M. Hemeda, A.M. Mohamed, J. Supercond. Nov. Magn. **33**, 2521–2525 (2020)
55. M.A. Hamad, O.M. Hemeda, H.R. Alamri, A.M. Mohamed, J. Mater. Res. Technol. **11**, 1356–1361 (2021)
56. M.A. Hamad, O.M. Hemeda, H.R. Alamri, A.M. Mohamed, J. Low Temp. Phys. **202**, 121–127 (2021)
57. M.A. Hamad, J. Supercond. Nov. Magn. **28**, 3111 (2015)
58. M.A. Hamad, J. Supercond. Nov. Magn. **27**, 1777 (2014)
59. A.H. El-Sayed, M.A. Hamad, J. Supercond. Nov. Magn. **32**, 1447 (2019)
60. H.R. Alamri, S.M. Elghnam, O.M. Hemeda, M.A. Hamad, Phys. Solid State **63**, 1332–1336 (2021)
61. M.A. Hamad, J. Supercond. Nov. Magn. **31**, 337 (2018)
62. M.A. Hamad, Process. Appl. Ceram. **11**, 225–229 (2017)
63. M.A. Hamad, Int. J. Thermophys. **34**, 1158–1165 (2013)
64. M.A. Hamad, Int. J. Thermophys. **36**, 2748 (2015)
65. M.A. Hamad, Int. J. Thermophys. **34**, 214 (2013)
66. M.A. Hamad, J. Adv. Ceram. **2**, 308–312 (2013)
67. A.H. El-Sayed, M.A. Hamad, J. Supercond. Nov. Magn. **31**, 4167–4171 (2018)
68. M. A. Hamad, O. M. Hemeda, H. M. Alamri, A. M. Mohamed, **33**, 3853–3856 (2020)
69. M.A. Hamad, J. Supercond. Nov. Magn. **28**, 2525–2528 (2015)
70. M.A. Hamad, J. Supercond. Nov. Magn. **28**, 3365 (2015)
71. M.A. Hamad, J. Supercond. Nov. Magn. **29**, 2867–2871 (2016)
72. M.A. Hamad, J. Supercond. Nov. Magn. **27**, 2569 (2014)
73. M.A. Hamad, J. Supercond. Nov. Magn. **28**, 3329–3333 (2015)
74. M.A. Hamad, J. Adv. Dielect. **3**, 1350008 (2013)
75. M.A. Hamad, J. Supercond. Nov. Magn. **28**, 2223 (2015)
76. A.H. El-Sayed, M.A. Hamad, J. Supercond. Nov. Magn. **31**, 4091–4094 (2018)
77. M.A. Hamad, H.R. Alamri, M.E. Harb, J. Low Temp. Phys. **204**, 57–63 (2021)
78. M.A. Hamad, J. Supercond. Nov. Magn. **27**, 269–272 (2014)
79. M.A. Hamad, J. Adv. Dielect. **4**, 1450026 (2014)
80. M.A. Hamad, Process. Appl. Ceram. **10**, 33 (2016)